

Lattice QCD with mixed actions

UKQCD Collaboration, K.C. Bowler, B. Joó, R.D. Kenway, C.M. Maynard and R.J. Tweedie

School of Physics, The University of Edinburgh, Edinburgh EH9 3JZ, UK

ABSTRACT: We discuss some of the implications of simulating QCD when the action used for the sea quarks is different from that used for the valence quarks. We present exploratory results for the hadron mass spectrum and pseudoscalar meson decay constants using improved staggered sea quarks and HYP-smearred overlap valence quarks. We propose a method for matching the valence quark mass to the sea quark mass and demonstrate it on UKQCD clover data in the simpler case where the sea and valence actions are the same.

KEYWORDS: lat, chl.

Contents

1. Introduction	1
1.1 Matching the quark masses	3
2. Overlap valence quarks on a staggered sea	6
2.1 Smearing	7
2.2 The light hadron spectrum	7
2.3 Charm Physics	10
3. Conclusions	11

1. Introduction

Solving lattice QCD to high precision requires the use of light dynamical quarks. Ginsparg-Wilson fermions have the correct chiral and flavour symmetries. However, they are computationally expensive compared to improved staggered quarks. In the $N_f = 2 + 1$ improved staggered programme the square root of the fermion determinant is employed to reduce the number of dynamical flavours from four to two for the up and down quarks, and the fourth root is taken to reduce the number of flavours from four to one for the strange quark [1]. Ensembles of gauge field configurations are then generated with these fractional power determinants as weight factors. There is no known local action to which this model corresponds. We define a mixed action as one where the action used to generate the ensemble of gauge configurations, or sea quark action, is different from the valence quark action used to determine hadronic observables on those configurations. Current $N_f = 2 + 1$ improved staggered simulations have a mixed action because the four-flavour staggered Dirac operator is used to generate the valence quark propagators rather than a local operator equivalent to that used in the ensemble weight. Unless a local operator can be found such that

$$\det D_{\text{local}} \equiv (\det\{D_{\text{st}} + m\})^{1/2} \quad (1.1)$$

mixed actions are inevitable in the improved staggered programme. The Chebyshev polynomial approximation to the square root of $(D_{\text{st}} + m)$ is not the required operator as it has been shown to be non-local [2, 3, 4]. That $(D_{\text{st}} + m)^{1/2}$ is non-local does not imply that D_{local} does not exist, but serves as a warning, since the obvious candidate for such an operator fails.

In the rest of this paper we assume that some D_{local} exists so that the improved staggered ensembles are generated with an action in the same universality class as QCD. We consider the case where the valence quark action is manifestly different from that

of the sea and we choose the valence action that has the best chiral properties, that is, overlap valence quarks on an improved staggered sea. In [5] a local Symanzik action and the corresponding low-energy chiral effective Lagrangian are constructed for a general Ginsparg-Wilson valence action with Wilson sea quarks. Some of their considerations apply to more general mixed actions and, in particular, to overlap valence quarks on a staggered quark sea [6].

Neuberger's overlap operator [7] is given by

$$D_{\text{ov}}(\mu) = \frac{1}{2} [1 + \mu + (1 - \mu) \gamma_5 \epsilon(H_W(-\rho))] \quad (1.2)$$

where H_W , is the Hermitian Wilson operator

$$H_W(-\rho) = \gamma_5 D_W(-\rho) \quad (1.3)$$

with mass parameter $0 \leq \rho \leq 2$, and $\epsilon(H_W)$ is the matrix sign function of H_W . The mass parameter μ is related to the bare quark mass am_q through

$$\mu = \frac{am_q}{2\rho} \quad (1.4)$$

although we will ignore this below and write $D_{\text{ov}}(m_0)$. The expectation value of some observable \mathcal{O} in a model where the ensemble has been generated as $2 + 1$ flavours of staggered quarks, with overlap valence quarks is

$$\begin{aligned} \langle \mathcal{O} \rangle = & \frac{1}{Z} \int \mathcal{D}U (\det \{D_{\text{st}}[U] + m_{ud}\})^{1/2} (\det \{D_{\text{st}}[U] + m_s\})^{1/4} e^{-S_g[U]} \\ & \times \mathcal{O} \left[\frac{\delta}{\delta \bar{\eta}_i}, \frac{\delta}{\delta \eta_i}, U \right] e^{-\bar{\eta}_i \{D_{\text{ov}}[U](m_i)\}^{-1} \eta_i} \Big|_{\bar{\eta}_i = \eta_i = 0}, \end{aligned} \quad (1.5)$$

where U are the gauge fields, Z is the partition function, $\{\bar{\eta}_i, \eta_i\}$, $i = 1, \dots, N_f$, are the valence quark sources and S_g is the gauge action. D_{ov} is positive and bounded from below by the valence quark masses m_i , assuming $m_i > 0$. The expectation values are equal to those of a local field theory with action given by

$$\begin{aligned} S = & S_g[U] + \sum_{l=ud} \bar{\chi}_l (D_{\text{local}}[U] + m_{ud}) \chi_l + \bar{\chi}_s (D_{\text{local}}[U] + m_s) \chi_s \\ & + \sum_i \bar{q}_i D_{\text{ov}}[U](m_i) q_i + \phi_i^+ D_{\text{ov}}[U](m_i) \phi_i \end{aligned} \quad (1.6)$$

where the χ fields are the one-component staggered sea quark fields, and the q fields are the overlap valence quark fields. The ϕ fields are pseudofermion sea fields introduced to cancel the determinant of the overlap operator [8]. For practical purposes the model can be regarded as having an exact $SU(N_f|N_f)_L \otimes SU(N_f|N_f)_R \otimes U(1)_V$ symmetry when $m_i = 0$ for $i = 1, \dots, N_f$ [9]. Restricting to transformations only in the valence quark sector, the infinitesimal chiral rotation is given by

$$\begin{aligned} \delta q &= i\epsilon\tau\gamma_5 \left(1 - \frac{1}{2}D_{\text{ov}}\right) q \\ \delta \bar{q} &= i\epsilon\bar{q} \left(1 - \frac{1}{2}D_{\text{ov}}\right) \gamma_5\tau \end{aligned} \quad (1.7)$$

and possesses the correct $U(1)_A$ anomaly and an index theorem.

For $N_f = 3$, this model is in the same universality class as QCD when the sea and valence quark masses are matched. At non-zero lattice spacing, the separate chiral symmetries for sea and valence quarks ensure that the lightest pseudoscalar meson mass vanishes at $m_{\text{val}} = m_{\text{sea}} = 0$. This implies that the bare quark masses are related by

$$m_{\text{val}} = \zeta(a)m_{\text{sea}} \quad (1.8)$$

where $\zeta \rightarrow 1$ as $a \rightarrow 0$. To date $N_f = 2+1$ simulations with staggered valence and fractional determinants of the staggered sea [1] have set $\zeta(a) = 1$. However, it is not obvious that this is the appropriate matching condition for overlap valence quarks on a staggered sea (or, for that matter, for staggered valence quarks).

1.1 Matching the quark masses

To match the sea and valence quark masses to their experimental values one would have to find an experimentally known hadronic state whose mass depends strongly on the sea quark mass. In principle, the η' is one such hadron. The sea quark mass could be tuned until the η' has the correct experimental mass, whilst tuning the valence quark mass of the flavour non-singlet pseudoscalar meson to the pion. In practice, this is rather difficult, as the η' requires very high statistics calculations. An alternative would be to relate the bare sea and valence quark masses to each other via equation (1.8), and then tune the flavour non-singlet mesons to their experimental values in the usual way.

When the sea quark mass is infinite, *i.e.* quenched, then Bardeen *et al.* [10, 11] have demonstrated numerically that the model violates unitarity. We extend this analysis for finite sea and valence quark masses and show the same unitarity violation occurs when $m_{\text{val}} < m_{\text{sea}}$. Our results suggest a criterion for matching the sea and valence quark masses. The quark masses can be tuned by varying the valence quark mass to see when these partially quenched pathologies appear for a given sea quark mass. This determines when the valence quark is lighter than the sea quark.

Bardeen *et al.* [10, 11] show that the scalar correlator,

$$C_{SS}(t) = \sum_{\vec{x}} e^{-\vec{p}\cdot\vec{x}} \langle \bar{\psi}(x)\psi(x)\bar{\psi}(0)\psi(0) \rangle \quad (1.9)$$

is sensitive to this quenched pathology, because it couples to an $\eta' - \pi$ intermediate state. Shown in figure 1 are two of the diagrams which contribute to the η' propagator. Diagram a), the ‘‘hairpin’’, has a negative coefficient. In full QCD, diagram b), with a series of vacuum bubbles, cancels the effect of the hairpin diagram, so there is no negative contribution. In quenched QCD, only the hairpin diagram contributes, so the intermediate $\eta' - \pi$ state couples with a negative spectral weight. This gives the scalar correlator a negative value.

In partially quenched QCD the situation is more complicated. The bubble in diagrams b) depends only on the sea quark mass, whereas the connected quark-flow lines depend only on the valence quark mass. Heuristically at least, the size of the contribution from diagrams b) can be thought of in the following way. When the sea quark mass is smaller than

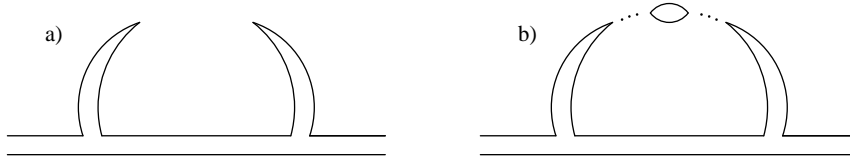


Figure 1: Quark-flow diagrams contributing to the η' propagator.

the valence quark mass, diagrams b) have a larger positive contribution than the negative contribution from diagram a). When the sea quark mass is heavier than the valence quark mass, diagram b) has a smaller contribution than a), which means the $\eta' - \pi$ intermediate state couples to the scalar correlator with a negative weight. By monitoring the sign of the scalar correlator as the valence quark mass is varied it should be possible to match the sea and valence quark masses.

To demonstrate this method, we examined the scalar correlator on the UKQCD $N_f = 2$ clover data sets [12, 13], where the sea and valence quarks have the same action. So whether the valence quark mass is heavier or lighter than the sea is known. This data was generated with the Wilson plaquette gauge action and the clover quark action, where the coefficient of the Sheikholeslami-Wohlert term [14] was determined non-perturbatively [15]. For all data sets $\beta = 5.2$ and the volume is $L^3 \times T = 16^3 \times 32$. The values of the hopping parameter for the sea and valence quark masses, and the number of configurations are shown in Table 1.

The relatively poor signal-to-noise ratio for the scalar correlator implies the need for a large number of configurations. To improve the statistical resolution, we used a ratio of correlation functions, as the statistical fluctuations are correlated. In particular, we considered the ratio

$$R(t) = \frac{C_{PP}(t) - C_{SS}(t)}{C_{PP}(t)} \quad (1.10)$$

where PP denotes the pseudoscalar correlator. At large times

$$\lim_{t \rightarrow T/2} R(t) = 1 - \frac{A_{SS}}{A_{PP}} \frac{e^{-m_S t} + e^{-m_S(T-t)}}{e^{-m_P t} + e^{-m_P(T-t)}}. \quad (1.11)$$

At the mid-point of the lattice

$$R(T/2) = 1 - \frac{A_{SS}}{A_{PP}} e^{-\Delta m T/2} \quad (1.12)$$

where $\Delta m = m_S - m_P$ is the mass splitting between the scalar and pseudoscalar states. For a large enough lattice time extent, T , this ratio tends to unity at the mid-point.

However, when the valence quark mass is lighter than the sea quark mass, the $\eta' - \pi$ state couples to the scalar correlator with a negative weight. Furthermore, this contribution does not fall exponentially with time, and so it is not exponentially suppressed by the mass splitting between the pseudoscalar and scalar states. Thus, a signal for the valence quark mass being lighter than the sea is $R(t) > 1$. Figure 2 shows the ratio for different sea and valence quark masses. The open circle and filled square both have the sea and valence quark masses equal, and R tends to unity at large times. For the filled circles, $R > 1$ at

large times at the 2σ level, a signal for partial quenching, and indeed this data set has $m_{\text{val}} < m_{\text{sea}}$. This effect is clearly dependent on the sea quark mass, as the open and filled circles both have the same valence quark mass.

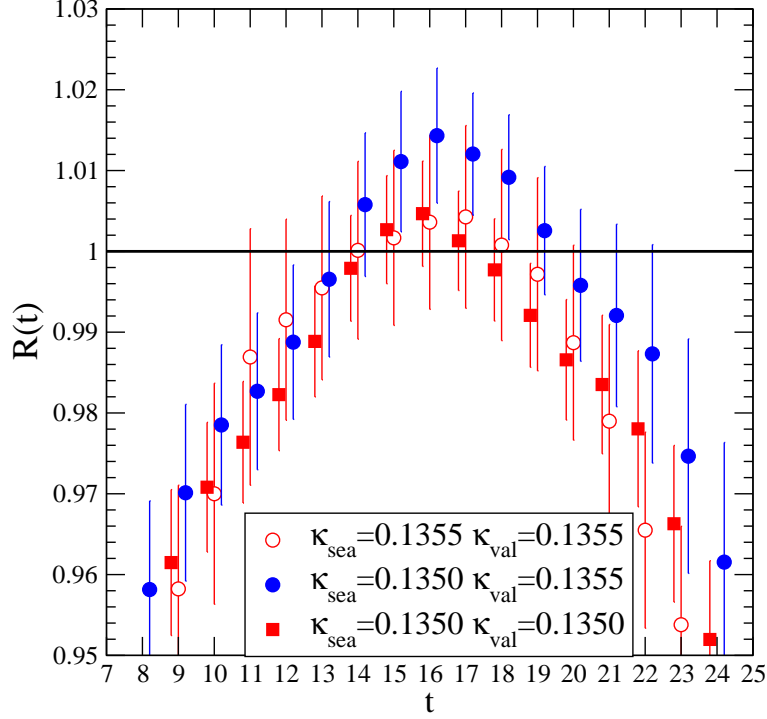


Figure 2: $R(t)$ in equation (1.11) versus Euclidean time, t .

κ_{sea}	κ_{val}	Nconfig	$m_{\text{val}} : m_{\text{sea}}$	A_{SS}/A_{PP}
	0.1340	202	>	0.6(1)
0.1350	0.1345	202	>	190(50)
	0.1350	202	=	0.0(2)
	0.1355	202	<	-0.00015(5)
0.1355	0.1350	208	>	1.2(2)
	0.1355	208	=	0.0(1)
	0.1355	141	>	1.5(5)
0.1365	0.1365	141	=	5.0(10)
	0.1380	141	<	-0.00014(14)
	0.1365	137	>	0.06(4)
0.1380	0.1380	137	=	0.0(1)
	0.1395	137	<	-0.003(2)

Table 1: UKQCD dynamical clover ($N_f = 2$) data sets for $\beta = 5.2$.

Also shown in Table 1 is the result of fitting equation (1.11) to the data. Clearly the ratio A_{SS}/A_{PP} is not a very well-determined quantity. However, it seems clear that this ratio being negative is a signal at the $1 - 2\sigma$ level that the data is partially quenched.

Figure 3 shows both the scalar correlator and the ratio (1.11). At lighter quark mass and with fewer configurations, the fit results become rather dependent on the fit range chosen, but combining the fit information and examining these plots, it is clear that for $\kappa_{\text{sea}} = 0.1356$, $\kappa_{\text{val}} = 0.13580$ there is a signal for the negative weight state, and for $\kappa_{\text{val}} = 0.1356$ this signal is absent.

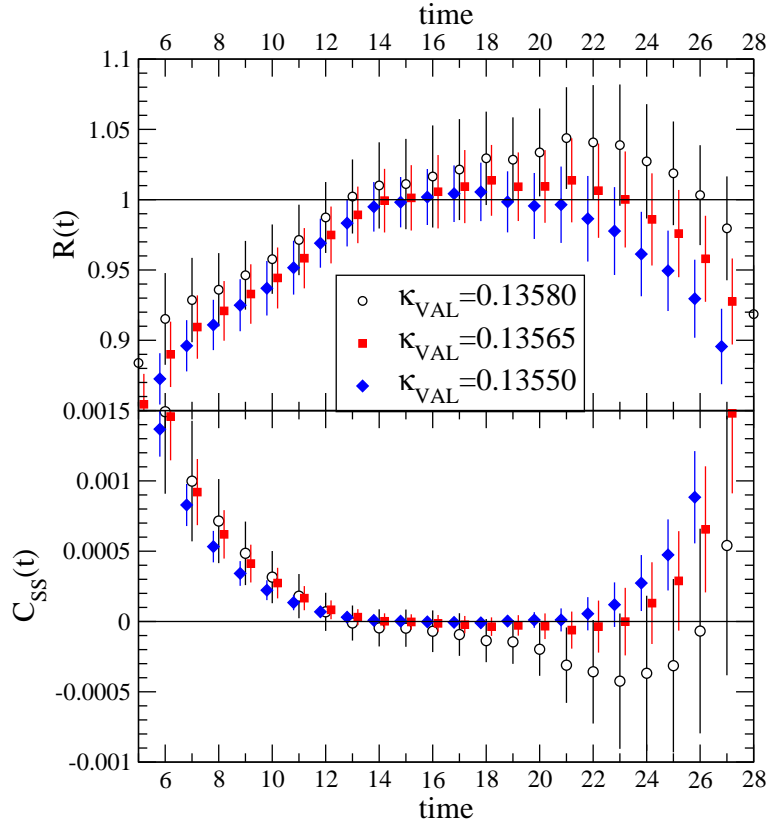


Figure 3: $R(t)$ and $C_{SS}(t)$ versus t for $\kappa_{\text{sea}} = 0.1365$.

A precise matching of the sea and valence quark masses will be difficult to achieve, because the signal for the scalar ground state at large times for light quarks seems to disappear into the noise. When the valence quark mass is lighter than the sea, the signal for the negative weight $\eta' - \pi$ state is fairly strong. However, our results suggest that it is possible, in principle, (equivalently with very high statistics) to match the valence and sea quark masses. This is necessary to make sense of simulations with mixed actions when at least one of the sea or valence quark masses is outwith the chiral regime and matching to chiral perturbation theory is problematic.

2. Overlap valence quarks on a staggered sea

We have performed an exploratory study of overlap valence quarks on the MILC $N_f = 2 + 1$ improved staggered configurations [16]. We measure the simplest states of the light hadron spectrum, mesons and baryons, and the pseudoscalar decay matrix element for

both light and heavy-light states. Due to a lack of computational resources, the number of configurations analysed was small, which prevented any realistic attempt at matching the sea and valence quark masses as described in the previous section.

2.1 Smearing

The overlap operator is only local for gauge configurations which are “smooth enough” [17]. The MILC configurations we used have a lattice spacing of $a \sim 0.125$ fm and so are relatively coarse. Smoothing the gauge configurations should improve the localisation of the overlap operator. Moreover, smoothing the gauge fields by “HYP-smearing” [18] can improve the spectral properties of the Wilson-Dirac operator [19], which reduces the amount of computation required in the solver used to apply $\epsilon(H_W)$. Indeed, HYP-smearing the gauge configuration does speed up the inversions. Furthermore, the low-lying eigenvalues of the staggered operator “mimic” the eigenvalue spectrum of the overlap operator when the configurations are smoothed in this way [20, 21, 22] suggesting that a smoothly behaved matching condition may exist for light quark masses.

To examine the effect of multiple iterations of HYP-smearing, we studied the quark-antiquark potential on 624 quenched UKQCD configurations at $\beta = 5.93$ with a volume of $16^3 \times 32$. The smearing parameters used were $\alpha_1 = 0.75$, $\alpha_2 = 0.60$, and $\alpha_3 = 0.35$ [18]. Planar Wilson loops were used to extract the quark-antiquark potential, which was fitted to

$$V(r) = V_0 + \sigma r - \frac{\kappa}{r} \quad (2.1)$$

Figure 4 shows the effect of multiple iterations of HYP-smearing on the string tension, σ . Repeated HYP-smearing quickly altered the short-distance behaviour, while the medium-to-long distance behaviour remained relatively unchanged for a small number ($\lesssim 3$) of iterations. The effect on the potential of smoothing configurations has been studied many times before, following the work of Teper [23], and recently an extensive study for different actions and different smearings has been carried out [24]. Our limited study agrees with these previous results.

2.2 The light hadron spectrum

The overlap propagator calculations were performed on ten configurations from each of two ensembles produced by the MILC collaboration [16]. One ensemble has $am_s = 0.05$, $am_l = 0.03$ and the other has $am_s = 0.05$, $am_l = 0.02$. Both have a lattice spacing $a \simeq 0.125$ fm and linear size $L \simeq 2.5$ fm. Three iterations of HYP-smearing were applied to each configuration. The overlap operator from the SZIN code [25] was then used to calculate propagators. These were created with seven different valence quark masses using the overlap multi-mass solver: four light and three heavy [26]. Some of these results have been previously reported in [27].

We performed simultaneous fits to three different correlators in order to extract the pseudoscalar meson mass (see figure 5). The fluctuations in the effective mass are larger than the apparent statistical errors, but this is probably due to underestimation of the variance on ten configurations.

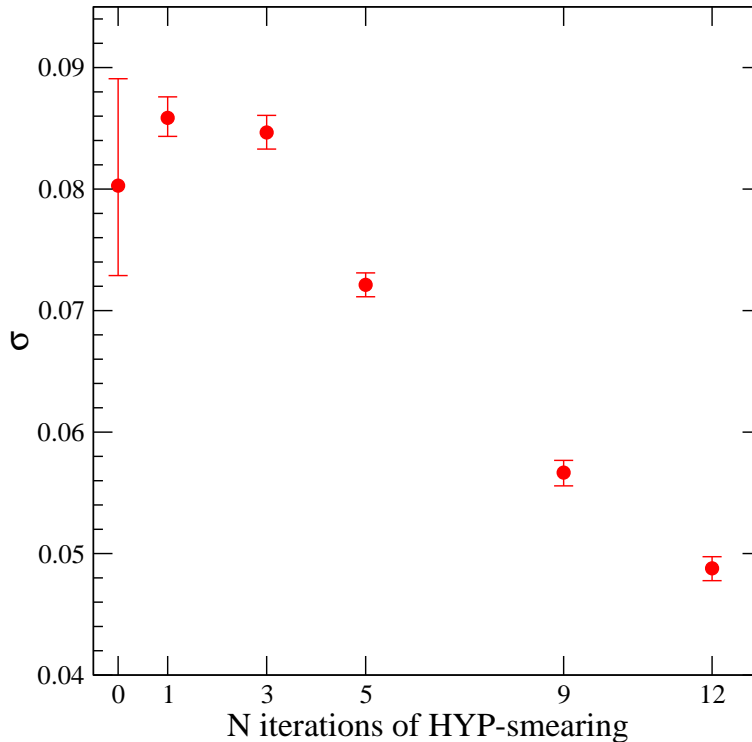


Figure 4: The effect of HYP-smearing on the long-range potential as measured by σ .

A partially quenched analysis was carried out, that is the sea quark mass was held fixed whilst varying the valence quark mass. Since we had multiple input valence masses, non-degenerate meson correlators could be constructed. Shown in figure 6 is the two-dimensional fit performed to $(aM_{PS})^2$ versus valence masses m_{q_1} and m_{q_2} , which allowed evaluation of the average u and d quark mass, \hat{m} , from

$$M_\pi^2 = B(m_{q_1} + m_{q_2}) + A = 2B\hat{m} + A \quad (2.2)$$

where M_π is the physical pion mass. This in turn allowed us to evaluate the strange quark mass, m_s , from

$$M_K^2 = B(m_s + \hat{m}) + A \quad (2.3)$$

where M_K is the physical kaon mass.

We also determined the masses of the nucleon and delta baryon. The signal for the nucleon mass is very clean. Figure 7 shows the effective mass of the nucleon for the two operators

$$\begin{aligned} N_1(x) &= \varepsilon_{ijk}(\psi_i^T C \gamma_5 \psi_j) \psi_k \\ N_2(x) &= \varepsilon_{ijk}(\psi_i^T C \gamma_4 \gamma_5 \psi_j) \psi_k. \end{aligned} \quad (2.4)$$

It is remarkable that we can see a signal for the negative parity partner of the nucleon on as few as ten configurations. This suggests that, despite their relative cost per propagator

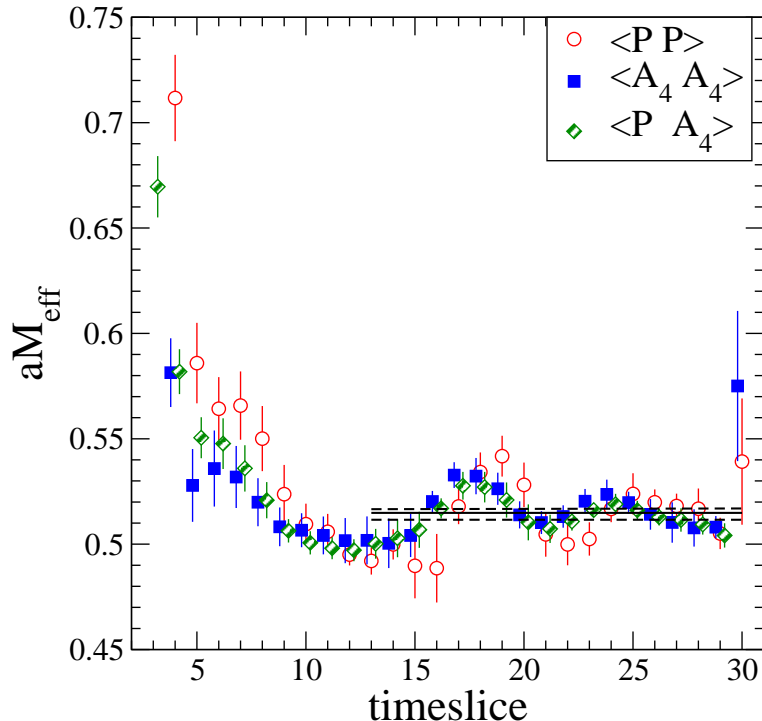


Figure 5: Pseudoscalar meson effective mass and simultaneous uncorrelated fit to three correlators ($P = \bar{q}\gamma_5 q$, $A_4 = \bar{q}\gamma_4\gamma_5 q$). The squares and diamonds are slightly offset horizontally for clarity.

compared with staggered quarks, overlap valence quarks maybe the most cost effective way to extract precision light baryon physics from improved staggered configurations.

Figure 8 shows the nucleon (upper plot) and decuplet (lower plot) masses versus the pseudoscalar meson mass squared. The lines are uncorrelated linear fits to the data. The values calculated by the MILC collaboration [16] on their corresponding full ensembles are shown by open symbols. Both the nucleon and decuplet baryon masses from the overlap operator are significantly lower although, *a priori*, we don't know how to match the horizontal scales. The cut-off effects for the different formalisms will be different and, unless the matching function in equation (1.8) is very different from one, this suggests that the cut-off effects for the overlap baryons are be smaller. The nucleon mass shows some sea quark mass dependence, but the decuplet mass shows no variation. With ten configurations and relatively heavy sea quark masses, any trend is hard to spot. In the lower plot, the vertical dashed-dotted line shows the estimate of the $\eta_{s\bar{s}}$ mass squared, as measured by the overlap operator on these configurations. The horizontal dotted line is the physical Ω^- mass in lattice units. Within large statistical uncertainties, this determination of the Ω^- mass at fixed lattice spacing agrees with the experimental value. Again, this may suggest that cut-off effects with overlap fermions are smaller than with staggered fermions, but, with data at only one lattice spacing, this remains speculation.

The pseudoscalar decay constant, f_{PS} , is defined as

$$f_{PS} = \frac{Z_A \langle 0 | A_4 | PS \rangle}{M_{PS}}. \quad (2.5)$$

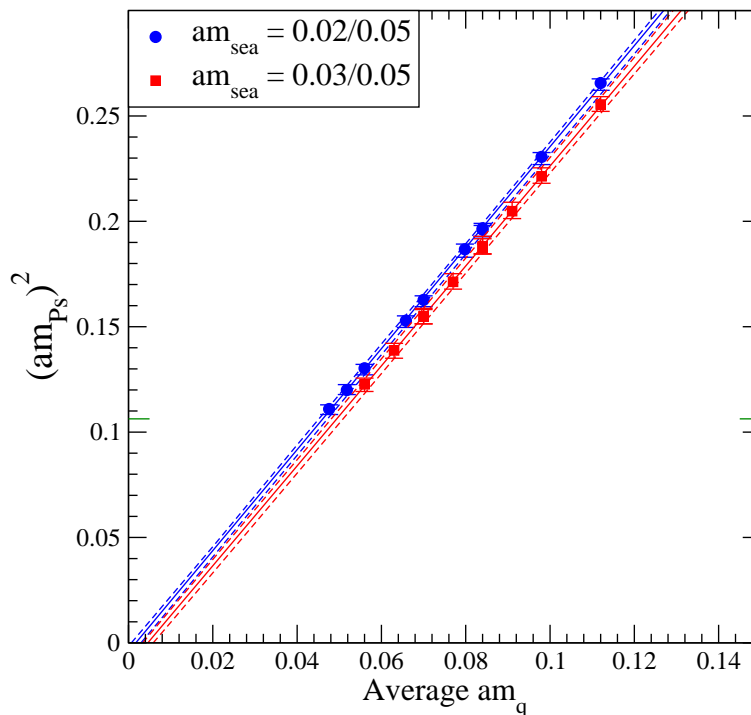


Figure 6: The square of the pseudoscalar meson mass vs bare overlap quark mass.

We obtain Z_A from the axial Ward identity

$$Z_A \langle \partial_\mu A_\mu \mathcal{O} \rangle = 2m_q \langle P \mathcal{O} \rangle \quad (2.6)$$

which we can express in terms of the pseudoscalar correlator, C_{PP} , and the pseudoscalar axial correlator, C_{PA_4} . $\langle 0|A|PS \rangle$ cancels in equation (2.5) and hence we require only C_{PP} to compute a renormalised f_{PS} . Once again, we performed a 2-d linear fit to the light non-degenerate pseudoscalars to calculate f_{PS} (see figure 9) and extracted the ratio of f_K/f_π (see table 2). The value increases slightly with decreasing light sea quark mass in the right direction to agree with experiment. This is also evident from the slight change of the gradient with sea quark mass in figure 9.

Sea Quarks	f_K/f_π	f_{D_s} (MeV)
$am_{\text{sea}} = 0.03/0.05$	1.03(3)	226(14)
$am_{\text{sea}} = 0.02/0.05$	1.08(4)	232(11)
Experiment [28]	1.22(1)	266(32)

Table 2: Pseudoscalar meson decay constants.

2.3 Charm Physics

Heavy quark propagators essentially come for free in the overlap propagator calculation through the use of a multi-mass solver. However, lattice artefacts are $\mathcal{O}(am_q)^2$ and the

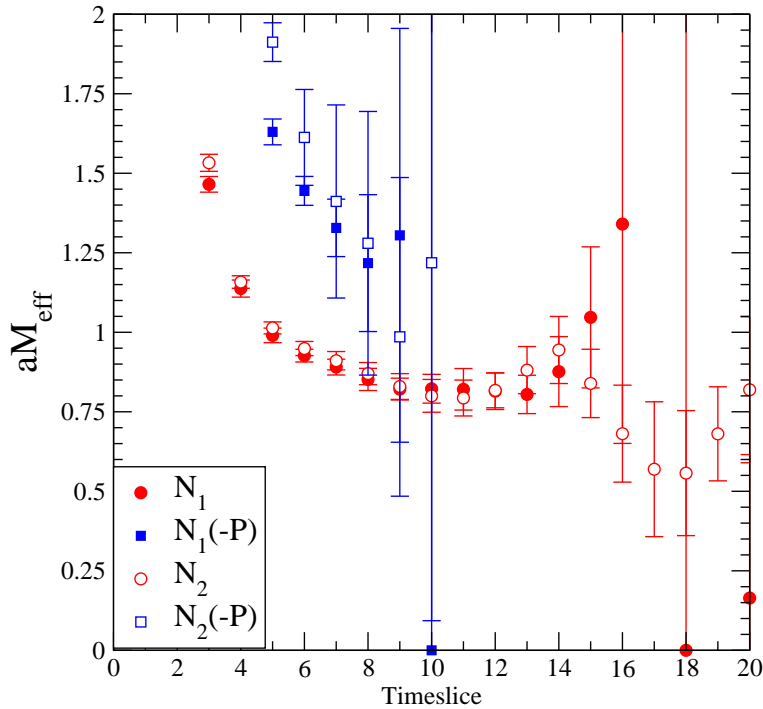


Figure 7: Nucleon effective mass for the heavier sea quarks, with $am_q = 0.056$ (equation 1.4). The square symbols show the negative parity excitation.

heaviest input valence quark mass used is $am_q = 0.84$, so $(am_q)^2 \sim 0.7$. With the lattice spacing of $a^{-1} \sim 1.5\text{GeV}$, the calculation is at best on the limit of simulating charm. Due to the rapid decay in Euclidean time, we require double precision. However, this does not slow the solver down appreciably, as we need substantially fewer re-orthogonalisations against the projected eigenvectors of H_W in the linear solver than in single precision.

These heavy quark propagators were used to calculate f_{D_s} (see table 2). The value of f_{D_s} increases with decreasing light sea quark mass, in the direction of the experimental value, as can be seen from the change of gradients in figure 10.

The short distance behaviour of the potential has been altered by repeated smearing. As heavy quarks in quarkonium feel the short distance potential, this repeated smearing may be a source of worry. Indeed, examining the heavy-heavy correlator for the heaviest quark mass we do not see the effective mass reaching a plateau. It might be expected that a heavy-light state feels the effect of the short distance potential less. Indeed the effective mass for the heavy-light correlator reaches a plateau. This suggests that the heavy-light states are not suffering so much from the modified short-distance behaviour. In future work we anticipate using fewer iterations of smearing.

3. Conclusions

While staggered quarks offer the most cost effective way of simulating light dynamical quarks today, they require us to use a mixed action formulation of QCD. Outside the chiral

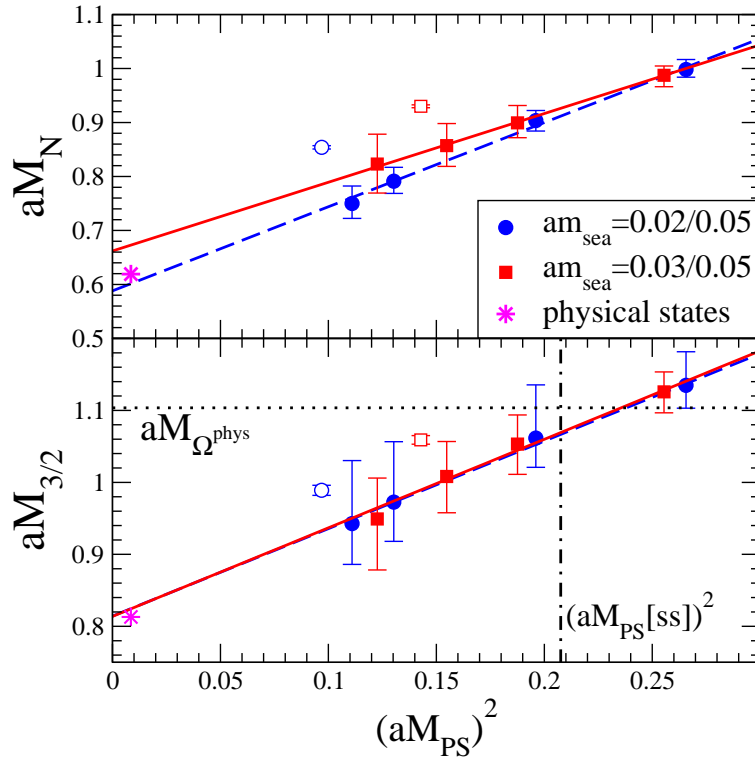


Figure 8: The nucleon and decuplet baryon mass versus $(aM_{PS})^2$ for the two ensembles. The open symbols show the baryon masses measured on the full ensemble with staggered valence quarks [16].

regime of both valence and sea quarks, it is necessary to implement a matching procedure for the quark masses for the model to be in the same universality class as QCD. (Within the chiral regime, the partially quenched results may be matched to chiral perturbation theory and thence to QCD low energy constants.) Indeed, we show numerically that the partially quenched theory with $m_{\text{val}} < m_{\text{sea}}$ has similar negative metric pathologies to those observed by Bardeen *et al.* in quenched QCD. In principle, this observation provides a matching condition, but, just like the alternative approach of determining m_{sea} by matching a flavour singlet quantity to experiment, suffers from poor signal-to-noise in practice. Despite these practical problems with matching, we obtain encouragingly good signals for flavour non-singlet hadron masses and decay constants using overlap valence quarks on a staggered sea quark ensemble. The potential gain from the simplicity of valence quarks with the correct flavour and chiral symmetries, together with the clean statistical signals, particularly for baryons, is good motivation for trying to improve on our exploratory attempts to match valence and sea quark masses.

Acknowledgments

We thank S. Sharpe for useful discussions.

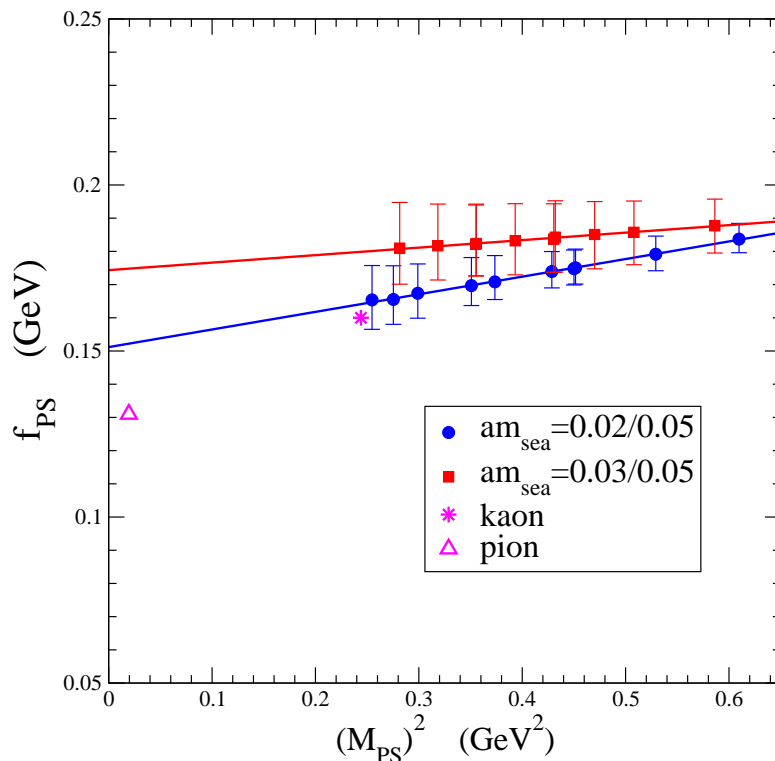


Figure 9: f_{PS} versus M_{PS}^2 for the two ensembles.

References

- [1] C. T. H. Davies *et al.*, *High-precision lattice QCD confronts experiment*, *Phys. Rev. Lett.* **92** (2004) 022001, [[hep-lat/0304004](#)].
- [2] B. Bunk, M. Della Morte, K. Jansen, and F. Knechtli, *Locality with staggered fermions*, *Nucl. Phys.* **B697** (2004) 343–362, [[hep-lat/0403022](#)].
- [3] B. Bunk, M. Della Morte, K. Jansen, and F. Knechtli, *The locality problem for two tastes of staggered fermions*, [hep-lat/0408048](#).
- [4] A. Hart and E. Muller, *The locality of the square-root method for improved staggered quarks*, *Phys. Rev.* **D70** (2004) 057502, [[hep-lat/0406030](#)].
- [5] O. Bar, G. Rupak, and N. Shoresh, *Simulations with different lattice Dirac operators for valence and sea quarks*, *Phys. Rev.* **D67** (2003) 114505, [[hep-lat/0210050](#)].
- [6] O. Bar, private communications.
- [7] H. Neuberger, *A practical implementation of the overlap-Dirac operator*, *Phys. Rev. Lett.* **81** (1998) 4060–4062, [[hep-lat/9806025](#)].
- [8] A. Morel, *Chiral logarithms in quenched QCD*, *J. Phys. (France)* **48** (1987) 1111–1119.
- [9] S. R. Sharpe and N. Shoresh, *Partially quenched chiral perturbation theory without ϕ_0* , *Phys. Rev.* **D64** (2001) 114510, [[hep-lat/0108003](#)].
- [10] W. A. Bardeen, A. Duncan, E. Eichten, N. Isgur, and H. Thacker, *Chiral loops and ghost states in the quenched scalar propagator*, *Phys. Rev.* **D65** (2002) 014509, [[hep-lat/0106008](#)].

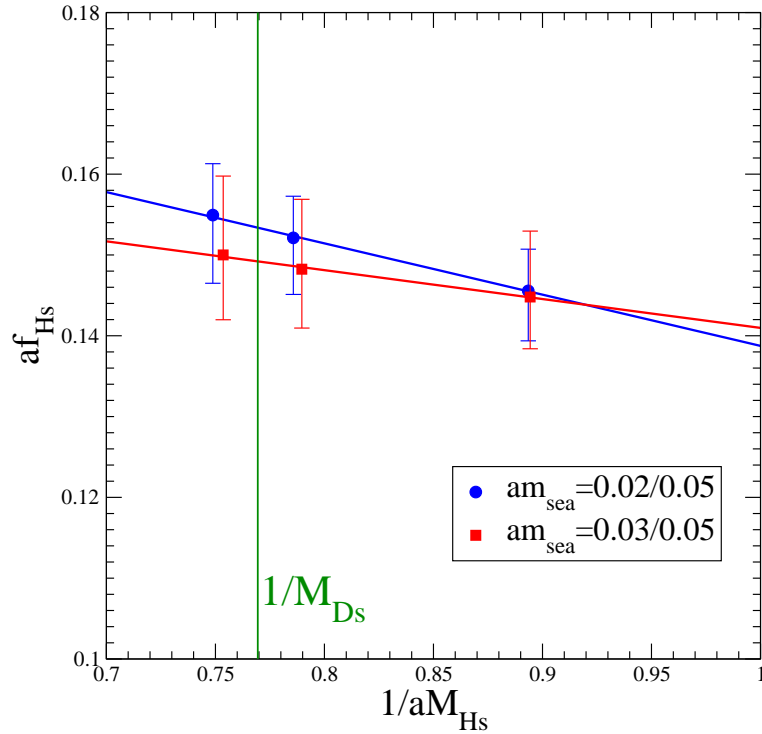


Figure 10: f_{H_s} vs inverse heavy-strange pseudoscalar meson mass.

- [11] W. A. Bardeen, E. Eichten, and H. Thacker, *Chiral lagrangian parameters for scalar and pseudoscalar mesons*, *Phys. Rev.* **D69** (2004) 054502, [[hep-lat/0307023](#)].
- [12] **UKQCD** Collaboration, C. R. Allton *et al.*, *Effects of non-perturbatively improved dynamical fermions in QCD at fixed lattice spacing*, *Phys. Rev.* **D65** (2002) 054502, [[hep-lat/0107021](#)].
- [13] **UKQCD** Collaboration, C. R. Allton *et al.*, *Improved Wilson QCD simulations with light quark masses*, *Phys. Rev.* **D70** (2004) 014501, [[hep-lat/0403007](#)].
- [14] B. Sheikholeslami and R. Wohlert, *Improved continuum limit lattice action for QCD with Wilson fermions*, *Nucl. Phys.* **B259** (1985) 572.
- [15] K. Jansen *et al.*, *Non-perturbative renormalization of lattice QCD at all scales*, *Phys. Lett.* **B372** (1996) 275–282, [[hep-lat/9512009](#)].
- [16] C. W. Bernard *et al.*, *The QCD spectrum with three quark flavors*, *Phys. Rev.* **D64** (2001) 054506, [[hep-lat/0104002](#)].
- [17] P. Hernandez, K. Jansen, and M. Luscher, *Locality properties of Neuberger’s lattice Dirac operator*, *Nucl. Phys.* **B552** (1999) 363–378, [[hep-lat/9808010](#)].
- [18] A. Hasenfratz and F. Knechtli, *Flavor symmetry and the static potential with hypercubic blocking*, *Phys. Rev.* **D64** (2001) 034504, [[hep-lat/0103029](#)].
- [19] T. DeGrand, A. Hasenfratz, and T. G. Kovacs, *Improving the chiral properties of lattice fermions*, *Phys. Rev.* **D67** (2003) 054501, [[hep-lat/0211006](#)].
- [20] S. Durr and C. Hoelbling, *Staggered versus overlap fermions: A study in the Schwinger model with $N(f) = 0, 1, 2$* , *Phys. Rev.* **D69** (2004) 034503, [[hep-lat/0311002](#)].

- [21] S. Durr, C. Hoelbling, and U. Wenger, *Staggered eigenvalue mimicry*, hep-lat/0406027.
- [22] S. Durr, C. Hoelbling, and U. Wenger, *A comparative study of overlap and staggered fermions in QCD*, hep-lat/0409108.
- [23] M. Teper, *Cooling and confinement in lattice gauge theory*, *Nucl. Phys.* **B411** (1994) 855–874.
- [24] S. Durr, *Gauge action improvement and smearing*, hep-lat/0409141.
- [25] <http://www.jlab.org/~edwards/szin/>.
- [26] S. J. Dong *et. al.*, *Chiral properties of pseudoscalar mesons on a quenched 20**4 lattice with overlap fermions*, *Phys. Rev.* **D65** (2002) 054507, [hep-lat/0108020].
- [27] **UKQCD** Collaboration, K. C. Bowler, B. Joo, R. D. Kenway, C. M. Maynard, and R. J. Tweedie, *Exploratory spectrum calculations using overlap valence quarks on a staggered sea*, hep-lat/0408043.
- [28] **Particle Data Group** Collaboration, S. Eidelman *et. al.*, *Review of particle physics*, *Phys. Lett.* **B592** (2004) 1.